ICLASS 2009, 11th Triennial International Annual Conference on Liquid Atomization and Spray Systems, Vail, Colorado USA, July 2009

Laser sheet imaging of high-velocity air atomised water sprays

P. L. Garlick*
Bournemouth, Dorset, UK

A. K. Jasuja
Cranfield University, Bedfordshire MK43 0AL, UK

Abstract

The flow structure in the near-nozzle region of a spray finishing atomizer is investigated. The analysis is based on flow visualization data obtained using laser sheet imaging. The liquid Reynolds number and aerodynamic Weber number are used to characterise the operating conditions. Both are varied in the range 10^3 to 10^4. An additional parameter, the momentum flux ratio M, is calculated for each test case. It is observed that for high values of the momentum flux ratio ($M > 20$) a film forms on the front face of the nozzle and the liquid flows towards the air in a radial direction. For low values of the momentum flux ratio ($M < 2$) a liquid jet is formed and the two streams do not meet until further downstream. For intermediate values of the momentum flux ratio ($2 < M < 20$) both flow regimes are present. The intact length of the liquid stream is also considered. Analysis of the entrainment process at the interface leads to the prediction that the intact length is inversely proportional to the mass flow ratio m. Close comparison is found between the observed and predicted lengths over the range $0.1 < m < 1.0$.

Introduction

The atomisation of a liquid jet by the action of a high-velocity coaxial air jet is a popular method for generating fine sprays. The technique is used in fuel combustors and spray coating devices, to name two examples. In both cases the detailed structure of the spray is important. Performance indicators such as power output and emissions, in the case of fuel combustors, and finish quality and transfer efficiency, in the case of spray coating devices, are strongly influenced by spray parameters such as droplet size distribution and pattern size and shape. There are well-established methods for measuring and predicting these parameters in the downstream, dilute region of the spray. Laser diffraction techniques can be used to measure droplet size, for example, and particle tracking techniques can be used to predict trajectories. However, the near-nozzle region is characterised by primary and secondary liquid break-up and droplet dispersion. Irregular shapes and spherical droplets co-exist in a dense spray zone. As a consequence both measurement and prediction are difficult. In the current work it is this region that is studied, with the aim of describing the features of the upstream flow that affect the characteristics of the overall spray.

For coaxial air atomizers of the type studied here the air pressure inside the air cap is typically above the critical pressure that produces sonic conditions at the exit. The convergent internal profiles that are commonly used generate an underexpanded annular jet. A pattern of oblique shock waves is formed in front of the air cap as the pressure of the jet adjusts to the ambient pressure. The supersonic air flow surrounds and interacts with a slow-moving liquid flow. The mechanism that generates small droplets from these initial conditions has been the subject of much research in recent years. See Lefebvre [1], for example, for a review, and Schmidt et al. [2] for a detailed description.

To visualize a flow field that contains fast-moving droplets it is necessary to utilise high-speed imaging methods. For high Weber number sprays such as those considered here average (SMD) diameters are typically of the order of 10μm with many droplets being as small as one micron. Very high speed imaging is required to freeze the motion of such small droplets. In the present work laser sheet illumination is used with a pulse duration of 10 ns. For objects moving at 100 m/s this is low enough to restrict the movement within the frame to one micron.

Experiments

The flow visualization work was conducted at the School of Engineering at Cranfield University. A new rig was constructed to support the atomizer, the camera and the laser equipment. The laser sheet was passed through a vertical slit in a plate mounted approximately 300 mm in front of the nozzle. The camera was mounted to the side, perpendicular to the laser sheet. The arrangement followed a similar approach to previous studies detailed in the paper of Rochaya et al. [3]. The camera used to capture the images was a TSI PowerView Plus 4MP. This has a 12-bit

*Corresponding author, pgarlick@dircon.co.uk

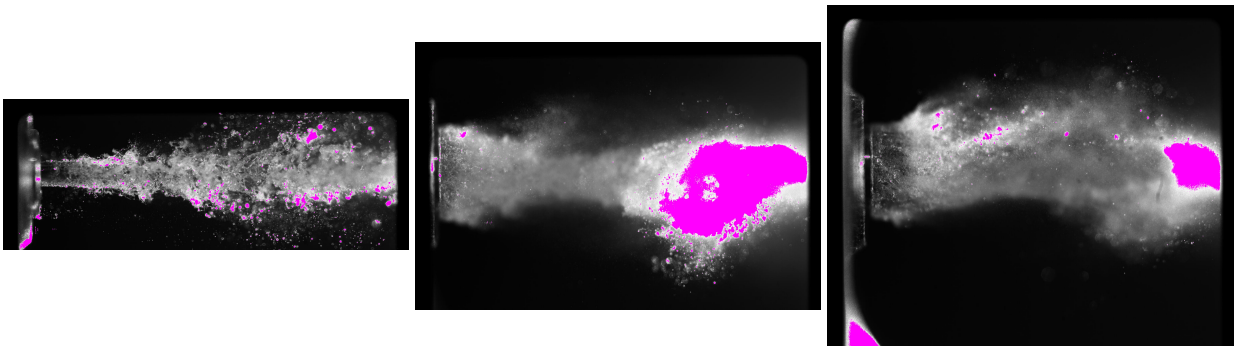

(a) jet mode: $\dot{m}_l = 590$ g/min, $p_a = 0.5$ bar and $d_l = 0.85$ mm (b) mixed mode: $\dot{m}_l = 190$ g/min, $p_a = 2.0$ bar and $d_l = 0.85$ mm (c) film mode: $\dot{m}_l = 110$ g/min, $p_a = 2.0$ bar and $d_l = 1.8$ mm

Figure 1: Images

intensity dynamic range and a resolution of four million (2048×2048) pixels. The camera was fitted with a 105 mm focal length lens and a 13 mm spacer. The light sheet was generated using conventional modular optics located at the exit of a New Wave Solo dual cavity laser. The maximum pulse energy was 50 mJ and the pulse duration was 10 ns.

Results

A total of thirty six tests were completed using water as the spray material. At each test condition, with the laser running at 7 Hz, seven consecutive images were acquired in the period of one second. In the course of the experiment it was found that some of the test conditions produced a jet flow in front of the nozzle. For these cases the camera was re-focused, moving the focal plane from the near edge of the front face of the nozzle to the axis of the nozzle.

The flow pattern in the near vicinity of the nozzle has an important bearing on the degree of atomisation measured downstream. Variations in droplet size distribution, including bimodal features, have been observed in previous studies [4] and attributed to the mode of the liquid flow. Three modes can be identified;

(i) jet mode—jet clearly visible, little radial flow,

(ii) mixed mode—jet visible, intermediate radial flow,

(iii) film mode—no jet visible, radial flow predominant.

Each set of seven images was studied in turn to categorize the mode of the liquid flow. The most appropriate mode for each combination of liquid flow rate $\dot{m}_l$, atomising air pressure p_a and nozzle size d_l was noted . Sample images, representative of the three modes, are shown in Figure 1. In Figure 1(a) a jet of equal diameter to the nozzle exit can be seen moving downstream along the axis. The jet surface remains undisturbed for approximately one exit diameter in front of the nozzle. The smooth flow in this region reflects the low level of turbulence in the emerging jet. Aerodynamic forces then begin to disrupt the jet. Short-wavelength perturbations appear on the surface and grow. The jet remains intact until approximately ten exit diameters in front of the nozzle. In Figure 1(b) a substantial proportion of the liquid flow is seen to be drawn across the front face of the nozzle. This flow meets the high velocity air flow at the outer edge of the front face, is atomised rapidly, and collapses back towards the axis, following the air stream. Meanwhile, the flow along the axis emerges from the surrounding flow at approximately three exit diameters in front of the nozzle. The combined flow meets with the fan air jets at the right hand side of the image, approximately 10 mm in front of the nozzle. In Figure 1(c) a larger proportion of the liquid flow is seen to be drawn across the front face of the nozzle. The thickness of the liquid film, indicated by the dark region immediately in front of the nozzle, is larger than that of the mixed mode case shown in Figure 1(b). The central jet is no longer visible. Instead there are voids in the flow visible close to the axis. In this image there is a significantly asymmetric distribution of the droplets, a feature noted in many of the lower liquid flow cases. This is evidence of an anti-symmetric, or flapping, mode of aerodynamic instability.

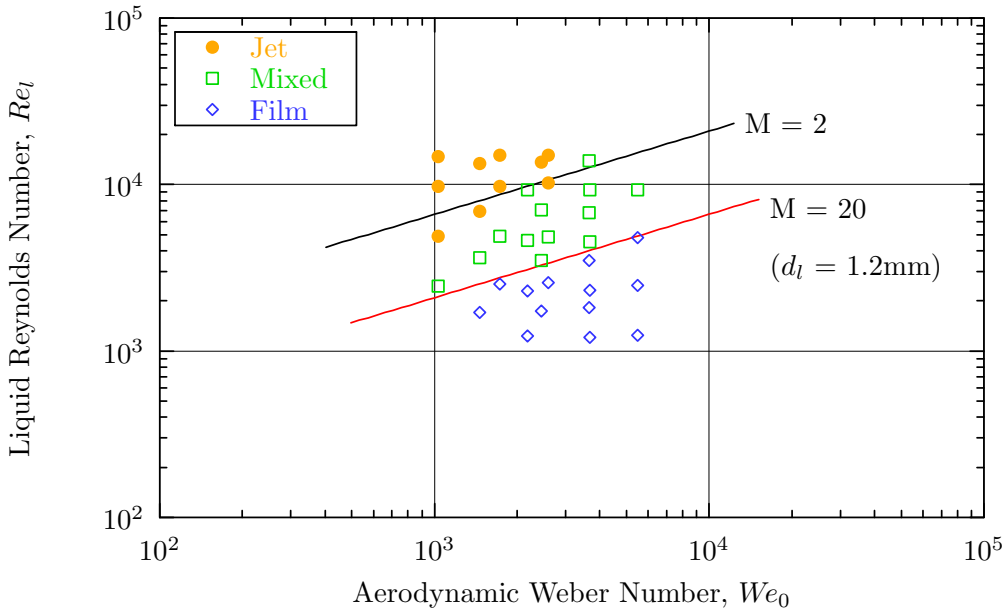

Figure 2: Water flow test results

Analysis

To characterise the type of spray under consideration it is useful to define a Reynolds number for the liquid flow and an aerodynamic Weber number for the air flow. The Reynolds number is a measure of the inertial force in the flow in comparison with the viscous force. The aerodynamic Weber number is a measure of the momentum force of the air flow in comparison with the surface tension force at the interface. The Reynolds number is defined as $Re_l = \rho_l U_l d_l / \mu_l$ where ρ_l is the liquid density, U_l is the liquid exit velocity, μ_l is the liquid viscosity and d_l is the exit diameter of the liquid nozzle. The aerodynamic Weber number is defined as $We_0 = \rho_g U_g^2 d_l / \sigma$ where ρ_g and U_g are the air exit density and velocity, d_l as before, and σ is the surface tension of the liquid. The length scale d_l accounts for the effect of the surface tension force in the case of the jet mode of liquid flow. For the film mode and mixed mode cases, where the film thickness is also an appropriate length scale, the use of d_l is justified on the basis that the film thickness is of the same order as the nozzle exit diameter. This observation, from images such as Figure 1(c), is consistent with the intact length predictions of Section .

The liquid physical properties are needed for the two dimensionless groups. Water at 20°C has a viscosity of 0.001 Pas. This value is used for the calculation of the liquid Reynolds Number. The surface tension of water at 20°C is 0.073 N/m. This value is used for the calculation of the aerodynamic Weber number.

For each combination of liquid flow rate $\dot{m}_l$, atomising air pressure p_a and nozzle exit diameter d_l the liquid Reynolds number and the aerodynamic Weber number are calculated. The Reynolds number is straightforward to calculate, using the relation $Re_l = 4\dot{m}_l / \pi d_l \mu_l$. The Weber number calculation requires the air exit velocity U_g and exit density ρ_g. These can be calculated using one-dimensional relations, taking the discharge coefficient for the air cap to be equal to 1.0. This is known to be a good estimate (within 5%) from measurements made in previous work. The form of the one-dimensional relations depends on whether the jet is sonic or subsonic at the air cap exit. For atomising air pressures above the critical pressure (0.90 bar for air discharging to atmosphere) the jet will be sonic. For lower pressures the jet will be subsonic.

An additional parameter, the momentum flux ratio per unit volume M, is calculated for each flow condition. This is defined as $M = \rho_g U_g^2 / \rho_l U_l^2$. This parameter has been used to distinguish break-up regimes in previous studies of co-axial atomizers (see, for example, Lasheras, Villermaux and Hopfinger [5] and Lasheras and Hopfinger [6]). It is a measure of the aerodynamic pressure of the air jet at the exit in comparison with the hydrodynamic pressure of the

liquid jet. In the recirculating region in front of the nozzle the balance between the two has a strong influence on the mode of the liquid flow. For low values of M the liquid meets little resistance to its axial motion and a jet is formed. A weak recirculation is established in the space between the liquid jet and the surrounding air jet. Atomisation is delayed until the two jets meet further downstream. As M increases the effect of the recirculation becomes more pronounced. The flow of the outer layer of the liquid jet is reversed and dragged back to the nozzle exit, then across the nozzle front face to be atomised directly. This is the mixed mode of liquid flow. For high values of M the recirculation extends all the way in to the axis. A central jet of air is established that opposes the axial motion of the liquid. The dynamic pressure of the returning air overcomes the dynamic pressure of the liquid jet and forces all of the liquid to flow in a radial direction. This is the film mode of liquid flow.

The liquid Reynolds number Re_l, the aerodynamic Weber number We_0 and the momentum flux ratio M are linked by the expression $Re_l = (We_0/M)^{1/2}(\rho_l \sigma d_l/\mu_l^2)^{1/2}$. For a given nozzle and spray material the three parameters are directly related. On a logarithmic plot of Re_l against We_0 contours of constant M are straight lines with gradient 0.5.

In Figure 2 the liquid Reynolds number Re_l is plotted against the aerodynamic Weber number We_0 for the complete set of water flow tests. The data points are colour-coded according to the mode of the liquid flow. In addition, two contours of constant M are shown. These are $M = 2$ and $M = 20$ for the mid-size nozzle ($d_l = 1.2$ mm). It can be seen that in the upper left region of the plot, where the momentum flux ratio M is less than 2, the mode of the liquid flow is the jet mode. In the lower right region, where M is greater than 20, the mode of the liquid flow is the film mode. For values of M between the lower limit $M_j(= 2)$ and the upper limit $M_f(= 20)$ the mode of flow is the mixed mode.

A small overlap between the jet mode and mixed mode regions is evident in Figure 2. A separate inspection of the results from each nozzle showed a weak dependence of the limits M_j and M_f on the nozzle size d_l. The lower limit M_j varied in the range 2–3, M_j increasing with nozzle size d_l. The upper limit M_f varied in the range 15–25, the limit again increasing with nozzle size d_l.

For the water flow tests the liquid Reynolds number Re_l and the aerodynamic Weber number We_0 both vary in the range 10^3 to 10^4. The moderate values of Re_l show that the internal liquid flow is laminar at the bottom end of the range moving to transitional and turbulent at the top end. The high values of We_0 show that the aerodynamic momentum force greatly outweighs the surface tension force. The break-up mechanism for high Weber number sprays is the growth of short wavelength disturbances leading to splitting of the bulk flow. This process can be seen most clearly in Figure 1(a).

Intact Length

An important parameter that affects the downstream characteristics of the spray is the liquid intact length, or break-up length. This is defined as the distance in front of the front face of the nozzle at which the continuous liquid flow splits into discrete pieces. These pieces may be spherical droplets, thin ligaments or irregular chunks. A schematic view of the geometry involved for the jet mode of liquid flow is shown in Figure 3. The jet is considered to form a cone-shaped feature in front of the nozzle. Entrainment from the surface of the cone, driven by the turbulent fluctuations in the surrounding air flow, transfers liquid from the intact jet to the discrete spray. The geometrical parameters that control the flow are the nozzle bore, d_l, the nozzle outer diameter, D_l, and the air cap bore, D_g. The air flow exits the air cap with velocity u_g, the liquid flow exits the nozzle with velocity u_l. The intact length in this case, denoted x_b, is the distance from the front face of the nozzle to the end of the cone.

For the film mode of liquid flow the geometry is different. A schematic view is shown in Figure 4. In this case a disk is considered to form in front of the nozzle. Recirculation in front of the disk prevents further axial motion. Entrainment occurs at the cylindrical surface of the disk. The intact length x_b is the thickness of the disk.

The aim of this section is to develop expressions for predicting the intact length x_b for both jet and film modes. In order to do so a representative velocity u_e is defined to describe the liquid velocity at the interface. Continuity of mass is used to link this velocity to the mass flow rate through the nozzle $\dot{m}_l$ and the area of the interface A. For convenience, a mass flow ratio m is defined such that $m = \dot{m}_g/\dot{m}_l$, where $\dot{m}_g$ is the mass flow rate of air through the air cap. The air velocity u_g is considered to comprise a mean component, U_g, and a fluctuating component u'_g;

$$u_g = U_g + u'_g$$

The liquid velocity u_l is decomposed in a similar way. For the case of laminar flow through the nozzle the fluctuating

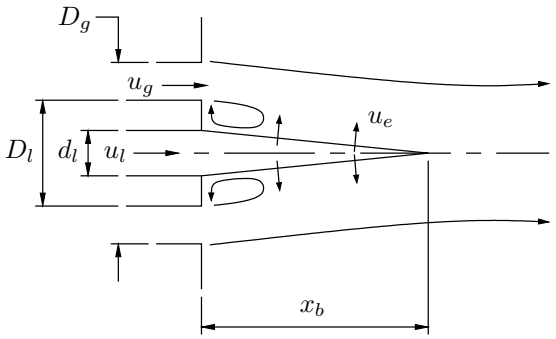

Figure 3: Schematic diagram of jet mode

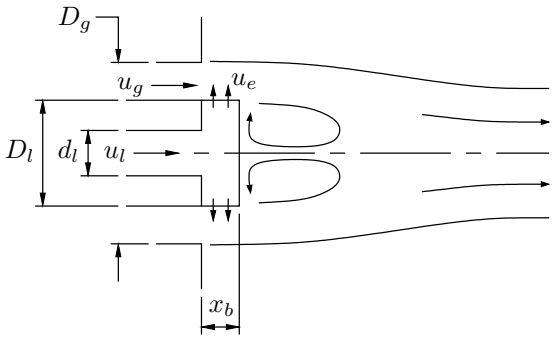

Figure 4: Schematic diagram of film mode

component u_l' is zero and the liquid velocity u_l is equal to the mean velocity U_l.

To close the expressions a link is needed between the entrainment velocity u_e and the mean air velocity U_g. This is provided by consideration of the balance of forces at the interface. On the basis that surface tension effects are small at the interface for high Weber number sprays such as these ($We_0 > 10^3$), the turbulent dynamic pressure of the air is said to induce a dynamic pressure in the liquid according to the following relation [5]

$$\rho_l \, u_e^2 = C_e \, \rho_g \, {u_g'}^2$$

where u_g' is the root-mean-square (r.m.s.) of the fluctuating air velocity component in the vicinity of the interface. The r.m.s value u_g' is related to the mean value U_g through the local turbulence intensity α;

$$u_g' = \alpha \, U_g$$

Measurements made for the case of equal-density coaxial jets give a value of $\alpha = 0.17$ (Rehab, Villermaux and Hopfinger [7]). The factor C_e in the dynamic pressure balance equation is determined from consideration of mass conservation for a single jet. Knowledge of the potential cone length for this case leads to a value of $C_e = 0.25$ [7].

In deriving the expressions for the intact length x_b it is useful to introduce the parameter D_h, equal to the hydraulic diameter $D_g - D_l$. Then, after substituting for u_e and u_g' in the dynamic pressure balance equation and supplying the area A for the cone-shaped geometry shown in Figure 3, the following expression is derived:

$$\frac{x_b}{D_h} = \frac{2}{\alpha \, m} \left(\frac{D_l}{d_l} \right) \sqrt{\frac{\rho_g}{\rho_l}}$$

This expression is valid for $x_b \gg d_l$, which is applicable for the jet mode case.

For the film mode case the area A is that of the disk-shaped geometry shown in Figure 4. The expression derived for this case is:

$$\frac{x_b}{D_h} = \frac{1}{\alpha \, m} \sqrt{\frac{\rho_g}{\rho_l}}$$

In both the jet mode case and the film mode case the intact length X_b ($= x_b/D_h$) is found to be inversely proportional to the mass flow ratio m. An increase in the air flow rate results in a reduction in the intact length. Conversely, an increase in the liquid flow rate results in an increase in the intact length. For the jet mode case a reduction in the nozzle diameter d_l results in an increase in the intact length (for the same mass flow ratio m). For the film mode case an increase in the nozzle outer diameter D_l results in a reduction in the intact length x_b (since, for constant mass flow, the hydraulic diameter D_h reduces as D_l increases).

To test the accuracy of the above expressions the intact length for each operating condition has been calculated. Comparisons have been made between the predicted intact lengths and the intact lengths observed in the corresponding photographs. An example for the film mode case is shown in Figure 5. These images show the effect of a change in the liquid mass flow rate, in this case from 100 g/min to 200 g/min. The mass flow ratio changes from $m = 0.5$ to

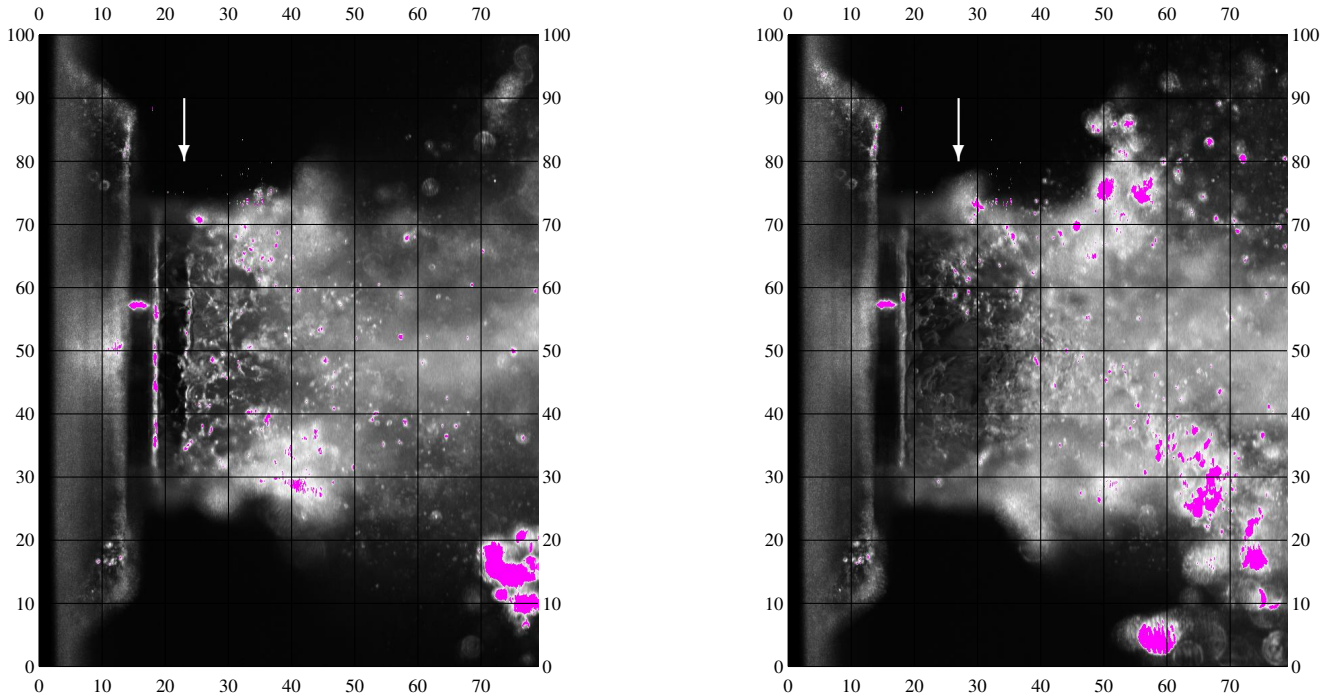

Figure 5: Intact Length; film mode (a) $m = 0.5$, $M = 190$, $X_b = 0.5$, $\dot{m}_l = 100$ g/min, $p_a = 0.5$ bar and $d_l = 1.8$ mm (b) $m = 0.2$, $M = 50$, $X_b = 0.9$, $\dot{m}_l = 200$ g/min, $p_a = 0.5$ bar and $d_l = 1.8$ mm

$m = 0.2$. The combined effect of the higher mass flow ratios, typical of the film mode of liquid flow, and the change in shape of the interface leads to markedly reduced intact lengths. The markers show the locations of the predicted lengths. For the lower flow rate case, Figure 5(a), the edge of the film can be clearly seen as the bright vertical line parallel to the front face of the nozzle. For the higher flow rate case, Figure 5(b), the edge of the film has a more ragged appearance. However, it is clear that the observed increase in thickness, approximately double in this case, is consistent with the predicted increase.

In the process of predicting values for the intact lengths the mass flow ratio m is calculated for each set of operating conditions. It is noted that, over the range of conditions tested, the mass flow ratio varies from a minimum of 0.1 to a maximum of 1.0. For the film mode cases the mass flow ratio is generally at the high end ($0.5 < m < 1.0$), consistent with the higher momentum flux ratio values. A few film mode cases have lower mass flow ratio values. The minimum value for a film mode case is $m = 0.2$. For the jet mode cases the mass flow ratio is always at the low end ($0.1 < m < 0.2$).

Discussion

The results shown in Figure 2 demonstrate the strong influence of the momentum flux ratio M on the mode of the liquid flow. When M is less than the lower limit $M_j = 2$ the liquid jet is substantially undisturbed and flows in an axial direction. When M is greater than the upper limit $M_f = 20$ the recirculating air flow forces the liquid to flow across the front face of the nozzle in a radial direction. At intermediate momentum ratios both modes are present.

In the work of Lasheras, Villermaux and Hopfinger [5] an estimate was given for the momentum flux ratio at which the inner liquid cone is chopped off by the recirculating air flow. Their limit $M_c \approx 35$, derived from their work on liquid propellant rocket engine applications, compares well with the limit $M_f \approx 20$ found in the present work.

The values of the two constants, C_e and α, that are used in the entrainment analysis are based on observations of similar flows. The close comparison of the predicted lengths with the observed lengths, as shown for example in Figure 5, demonstrate that the values obtained from the previous studies are applicable to the flow conditions

investigated here. Further improvement in the accuracy of the predictions could be made by careful measurement of the turbulence intensity in the vicinity of the entrainment region, to refine the value of α, and correlation of the intact length measurements for both film and jet mode, to refine the value of C_e.

References

[1] Arthur H. Lefebvre. *Atomization and Sprays*. Hemisphere Publishing Corporation, 1989.

[2] David P. Schmidt, Louis M. Chiappetta, Graham M. Goldin, and Ravi K. Madabhushi. Transient multidimensional modeling of air-blast atomizers. *Atomization and Sprays*, 13(4), Jul–Aug 2003.

[3] D. Rochaya, A. K. Jasuja, J. B. M. Pierce, and J. B. Moss. Combustion of bio-mass derived liquid fuels in gas turbines. In *20th Annual Confererence Proceedings*. ILASS-Europe, 2005.

[4] Ronen Harari and Eran Sher. Bimodal drop size distribution behaviour in plain-jet airblast atomizer sprays. *Atomization and Sprays*, 8(3), May–Jun 1998.

[5] J. C. Lasheras, E. Villermaux, and E. J. Hopfinger. Break-up and atomization of a round water jet by a high-speed annular air jet. *Journal of Fluid Mechanics*, 357:351–379, 1998.

[6] J. C. Lasheras and E. J. Hopfinger. Liquid jet instability and atomization in a coaxial gas stream. *Annual Review of Fluid Mechanics*, 32:275–308, 2000.

[7] H. Rehab, E. Villermaux, and E. J. Hopfinger. Flow regimes of large-velocity-ratio coaxial jets. *Journal of Fluid Mechanics*, 345:357–381, 1997.